Microscale study on dynamics of particles in slurry filtrated through porous media

D Sun[1]

Department Earth Science and Engineering, Imperial College London, London, UK SW7 2AZ

Abstract

In porous media, migration of particles in slurry is constrained, and most particles can be retained by the structure. As a result, the structure and topology of the porous media are altered, which, in turn, varies the fluid dynamics of both the fluid and particles. Clogging issues cause a reduction in flow by reducing permeability. The pore-clogging was predominantly determined by the size ratio between the opening of the pore throat and the diameter of the particles passing through. In this study, the fluid-particle flow is simulated numerically to study the dynamics of transport and retention of particles in a microscale porous medium. The determinant effects of the volume fraction of particles and stokes number were primarily investigated on particle clogging. Meanwhile, the dynamics of the particles and fluid field were studied to evaluate the permeability of the porous media due to clogging in a microscale analysis.

Keywords: porous media; particle filtration; particle dynamics; particle transport

1. Introduction

Particle filtration in porous media plays a key role in petroleum engineering, water resources, environmental engineering, and power engineering. In the oil industry, particulate suspension and filtration have a wide range of applications in both petroleum recovery and processing, such as the migration of fines and clay minerals during recovery, drilling fluid suspensions, well stimulation and fracturing suspensions, and propagation of ultra-dispersed catalyst in porous media for in-situ upgrading of heavy oil as a new and innovative technology [1, 2]. In addition, the mechanism of colloidal particle

[1] Corresponding author. E-mail address: d.sun@imperial.ac.uk.

migration in porous or fractured aquifers has aroused the interest the geoscientists in addressing certain issues that may affect the sustainability of the exploitation of groundwater resources [3]. Rough filters (course media filtration) were used as pre-treatment systems when the raw water contains a large number of suspended particles and organic matter [4]. Moreover, diesel particulate filters are widely used in vehicles as a piece of effective after-treatment equipment to physically remove the hazardous particulate matter from the exhaust gas flow [5,6].

Most research were focusing on the efficiency and sustainability of operations and treatments, looking at the permeability reduction of porous media and productivity damage due to clogging. The experimental results showed that injection of the real chlorinated secondary effluent from municipal sewage plants caused a significant decrease (> 80%) in permeability of porous medium within 3 days[7]. During the filtration process, particles can be carried along the filtrate and deposited within the filter medium thereby clogging and reducing the permeabilities of the porous media. This in turn affects the growth rate of the compact as well as the density and microstructure uniformity. [8] As each injected particle gets trapped, it alters the fluid flow field, which in turn alters the flow field for subsequent particles. Also, as particles are diverted away from the blocked pore throats, the concentration of particles passing through the open pore throats will increase. This in turn may lead to a rapid build-up of particles on these adjacent collectors until they are also clogged. Consequently, if the conditions of deposition are such as to encourage extensive particle bridging, this will eventually lead to a situation where particle bridging occurs across all the pore throats. If this occurs at, or near, the face of the filter bed, the particles will tend to deposit on each other, and the mode of filtration will change from deep bed filtration to "cake" formation [9] In principle, particle transport and clogging in porous media depend on various factors that generally fall into two categories: straining and non-straining. Particle straining is where particles are retained in pore throats that are too small to allow the particles to pass through; it is controlled solely by particle size and pore construction[10]. For particles with smaller diameters than the pore throat, non-straining, which depends on the particle flow, particle-porous media, and particle–particle interactions including electrostatic force, diffusion, multiparticle bridging, surface deposition, interception, inertia, and hydrodynamic force play a decisive role in transport[11].

Various numerical methods were applied to study particle transport in porous media. Kokubun et al. [12] employed the continuous method of the classical mixture theory under the condition that the Stokes Number was less than 1, where the particulate phase was described by the volumetric fraction occupied. Kim et al. [13] used the RANS equations for the fluid flow and tracked the particles with a Lagrangian method, Discrete Phase Model, with the interfacial solute transport phenomena modeled by an upscaled stochastic transport model, Spatial Markov model. Parvan et al. [14, 15] developed a Lattice Boltzmann method to systematically simulate particle clogging coupled with a Lagrangian method. Hyman et al. [16] calibrated an unscaled continuous time random walk approach for adventive transport based on an Ornstein-Uhlenbeck model for the particle velocities that accounts for the fracture-matrix coupling using a compound Poisson process. Su et al.[17] developed a new algorithm for particle pore-scale transport through the porous media with arbitrarily polyhedral mesh, where Navier-Stokes Equation was used to describe the continuous phase motion in the Eulerian framework, Discrete element method (DEM) to describe the particle-particle interactions, and RIGID to detect the contact state between particles with arbitrarily shaped pore walls. Meanwhile, a novel consistent fictitious domain method in the arbitrarily collocated polyhedral mesh was developed. Gray et al. [18] introduced a hybrid simulation model to calculate the hydrodynamic dispersion in the pore scale images of real porous media. A stochastic particle model for simulating the transport of a solute was coupled with a lattice Boltzmann algorithm to calculate the flow field. Kermani et al. [19] developed a combined lattice Boltzmann-smoothed profile method to explore the coupled mechanism governing the transport of colloids and their retention in porous media. These research demonstrated that the microscale mechanism of particle filtration in porous media can be investigated using the numerical method.

In this study, the non-straining scheme of particle filtration in porous media is numerically investigated when the particles are smaller than the pore throat. A microscale structure of porous media was built to study the dynamics of particle flow in slurries to understand the mechanism of particle clogging and multiparticle bridging in porous media. The effects of the fluid, structure of porous media, and particle diameters and concentrations on particle transport and retention are studied on the particle clogging in porous media.

2. Numerical method

The fluid-particle flow was simulated using Computational Fluid Dynamics (CFD)-discrete element method (DEM). The liquid phase was simulated by solving the Navier-Stokes equation. [20]

$$\frac{\partial \alpha_l \rho_l}{\partial t} + \nabla \cdot (\alpha_l \rho_l \overrightarrow{u_l}) = 0 \quad (1)$$

$$\frac{\partial \alpha_l \rho_l \overrightarrow{u_l}}{\partial t} + \nabla \cdot (\alpha_l \rho_l \overrightarrow{u_l} \overrightarrow{u_l}) = -\nabla \mathrm{p} + \nabla \cdot (\overrightarrow{\tau_l}) - \frac{1}{\alpha_l V_{\mathrm{cell}}} \cdot \left| \sum_i (\alpha_l \overrightarrow{F_{D,l}}) \right| \cdot \frac{\overrightarrow{u_l} - \overrightarrow{u_s}}{|\overrightarrow{u_l} - \overrightarrow{u_s}|} \quad (2)$$

where the stress tensor of the liquid $\overrightarrow{\tau_l} = (\lambda_l - (2/3)\mu_l)(\nabla \cdot \overrightarrow{u_l})\vec{I} + \mu_l\left((\nabla \overrightarrow{u_l}) + (\nabla \overrightarrow{u_l})^T\right)$.

DEM was used to trace the trajectory of particles. The governing equations of the translational and rotational motions of particles are as follows:

$$m \frac{d\overrightarrow{u_p}}{dt} = \overrightarrow{F_D} + \overrightarrow{F_p} + \overrightarrow{F_\tau} + \overrightarrow{F_c} \quad (4)$$

$$I \frac{d\overrightarrow{\omega_p}}{dt} = \overrightarrow{T_c} + \overrightarrow{T_r} \quad (5)$$

Where the forces *F* and torques *T* were predicted using the constitutive correlations in Table 1.

Table 1 Forces and torques impacted on particles [21, 22]

1. Drag force [23, 24],

$$\overrightarrow{F_D} = \frac{1}{8} C_D \rho_l \pi d_p^2 \left|\overrightarrow{u_l} - \overrightarrow{u_p}\right| \left(\overrightarrow{u_l} - \overrightarrow{u_p}\right)$$

$$C_D = \left(0.62 + \frac{4.8}{\sqrt{\mathrm{Re_p}}}\right)^2 \alpha_g^{2-\chi}$$

$$\chi = 3.7 - 0.65 \exp\left[-\left(1.5 - \log_{10}\mathrm{Re}_p\right)^2/2\right]$$

2. Reynolds number of particles,

$$\mathrm{Re_p} = \rho_l d_p \left|\overrightarrow{u_l} - \overrightarrow{u_p}\right| / \mu_l$$

3. Pressure gradient force,

$$\overrightarrow{F_p} = -\nabla p \cdot V_p$$

4. Viscous force [25],

$$\overrightarrow{F_\tau} = -(\nabla \cdot \vec{\tau}) V_p$$

5. Normal component of the contact force between particle i and particle j,

$$F_n = -k_n d_n - c_n(u_{n,i} - u_{n,j})$$

6. Tangential contact force,

$$F_t = \min\left\{\left|k_t \int_{t_{c,0}}^{t} (u_{t,i} - u_{t,j})dt + c_t(u_{t,i} - u_{t,j})\right|, \mu_c F_n\right\}$$

7. Torque due to friction at the contact point,

$$\overrightarrow{T_c} = \overrightarrow{\mathrm{r_c}} \times \overrightarrow{F_t}$$

8. Torque due to rolling friction [26],

$$\overrightarrow{T_r} = R_\mu k_n \Delta d_n \frac{\omega_{rel}}{|\omega_{rel}|} r_p$$

$$\overrightarrow{\omega_{rel}} = \frac{r_i \overrightarrow{\omega_i} + r_j \overrightarrow{\omega_j}}{r_i + r_j}$$

---

3. Simulation of particle filtration

Figure 1 shows the microscale structure of the porous medium used in this study, built by particles in a square lattice, where D_0 was the diameter of particles on the lattice and W was the distance between two such particles. The flow domain in this study was characterized as a wave channel as in the red box in Figure 1. The depth of the 3-D geometry in the direction vertical to the surface seen in Figure 1 was assumed as $D_0/4$ in this study. Therefore, the cross-section of this medium is the width of D_0 and depth of $D_0/4$. The width of the narrowest gap of the 2-D wave channel is 0.40 times of D_0. The slurry with particles carried by liquid flowed from the left to the right.

In the study, the density and viscosity of the liquid were 866 kg/m^3 and 1.23e^{-3} kg/m·s, respectively. The particle density was 829 kg/m^3. The particle diameter, d_p, was assumed in the range of $D_0/40$ to $D_0/5$, which was about 1/16 to 1/2 times of the gap width of the narrowest pore throat. Assume that D_0 = 200 μm. The mean velocity of slurry, a mixture of liquid and particles, was denoted as U_0, in this study.

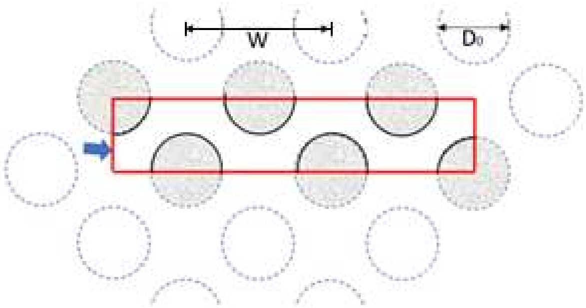

Figure 1. Microscale structure of the porous medium

3.1 Particle dynamics of single particles

As a single particle injected in the 2-D structure of porous media, the particle was carried by the liquid flowing along the wave channel of the porous medium. The particle in the porous medium was solely affected by the flow dynamics and porous structure. In Figure 2, the particles of D_0/40, D_0/20, D_0/10, and D_0/ 5 in diameter were simulated, as the single particle carried by the liquid passing through the porous medium. The initial location of particles is seen on the top of Figure 2-(a). Where from top to the bottom, the resident time of particles increased from 0 to 2.5 τ. The time intervals were τ and 0.5 τ, where, the characteristic time, $\tau \equiv D_0 / U_0$. It is observed from Figure 2-(a) that the flow positions of various particles were close, carried by a lower mass flow rate of liquid when Re = 0.4.

From Figure 2-(a) to (c) the mass flow rate of liquid increased. When Re = 4.0, the smaller particles moved ahead of the larger particles. When Re = 20, the largest particle, $d_p = D_0 /5$, was observed being left behind and wandering near the corner at the second wave.

In Figure 2-(d), the size of the pore throat was varied by reducing the distance between two packed cylindrical "particles", where W = 1.8 D_0. The liquid was assumed at the same mass flux as that in Figure 2-(b), whereas the large particles moved slower when W = 1.8 D_0 in Figure 2- (d) than those when W = 2.0 D_0 in Figure 2- (b). The instantaneous distance between the smaller particles in the diameter of D_0/40 and D_0/20 was simulated increased in the wave channel with a narrower gap in Figure 2-(d).

(a) W= 2.0 D_0, Re = 0.4 (t/τ = 0, 1, 2, 2.5)

(b) W= 2.0 D_0, Re = 4.0 (t/τ = 1, 2, 3, 4)

(c)W= 2.0 D_0, Re = 20 (t/τ = 1, 2, 3, 4)

(d) W= 1.8 D_0, Re = 3.6 (t/τ = 1, 2, 3, 4)

Figure 2. Single-particle flow in porous media.

Figure 3 shows the lateral displacement of each particle carried by the liquid varying with time. In Figure 3(a), when the mass flow rate of particles was lower, the lateral locations of all sizes of particles were close. The values of the lateral displacements of particles were higher than the liquid displacement at the mean velocity represented by the line at the unit gradient. This means that the velocity of the particles was higher than the mean velocity of the liquid, owing to the particles moving close to the center line of the wave duct where the local velocity is higher than the mean velocity of the liquid.

As the mass flow rate of the slurry increased from cases from Re = 0.4 in Figure 3(a) to Re = 4.0 in Figure 3(b), the gradient of particle displacements reduced close to the liquid gradient. The gradient of the larger particles at the diameter of $D_0/5$ was much lower than the others and the velocity of this large particle was much lower than the mean velocity of the fluid. As the mass flow increased further in

Figure 3(c) when Re = 40, the gradient of the lateral distance of particles reduced further, and the velocities of all sizes of particles were lower than the mean velocity of the liquid, U_0. It was observed that the particles biased further from the liquid flow field when the mass flow rate increased.

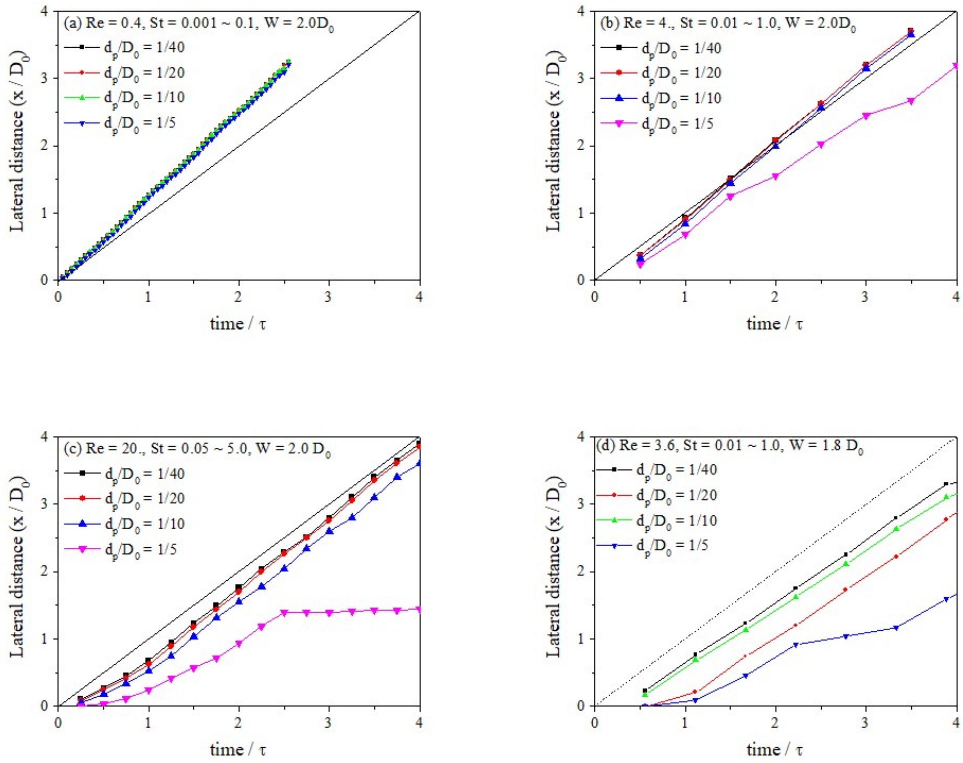

Figure 3 Lateral distance of single particle flow varying with time.

The size of the pore throat reduced in Figure 1-(d), where $W = 1.8\ D_0$. Using the same mass flux as in Figure 1-(b), the gradient of the particle distance reduced obviously. The lateral velocities of all sizes of particles were modelled less than the mean lateral velocity of the liquid. Therefore, the flow dynamics of particles is affected by the structure of the porous media.

3.2 Fluid dynamics of multiple particles

Figure 4 shows the transport of multiple particles in porous media. The diameter of the mono-sized particles varied from $D_0/20$, $D_0/10$ to $D_0/5$. The mass flow rate of slurries increased, where the Reynolds number varied from 0.4 to 4.0. The volume fraction of particles, α_s, was 5.0%. The left and right boundaries were assumed as the periodic boundary condition.

Figure 4 (d) shows the lateral component of the averaged velocity of particles varying with time. This averaged velocity was the velocity spatially averaged over all the particles in the flow region. Initially, the particles were uniformly distributed in the flow region, then accelerated by the liquid flow, hence the particle velocity increased to follow the liquid flow field. Gradually, the lateral mean velocity varied with the time at a pseudo-steady state. It is seen from the figure that, the velocity of smaller particles at the diameter of $D_0/20$ and $D_0/10$ varies little at this time resolution. The velocity of larger particles at the diameter of $D_0/5$ varied regularly with time, since the number of the large particles was less than the other two sizes of particles.

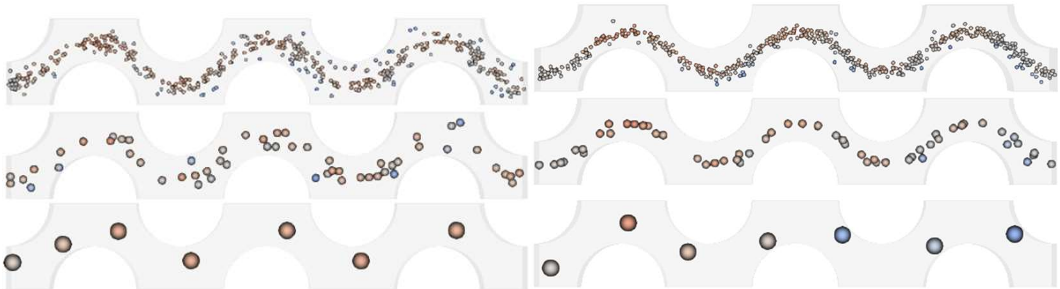

(a) Re = 0.4 (b) Re = 2.0

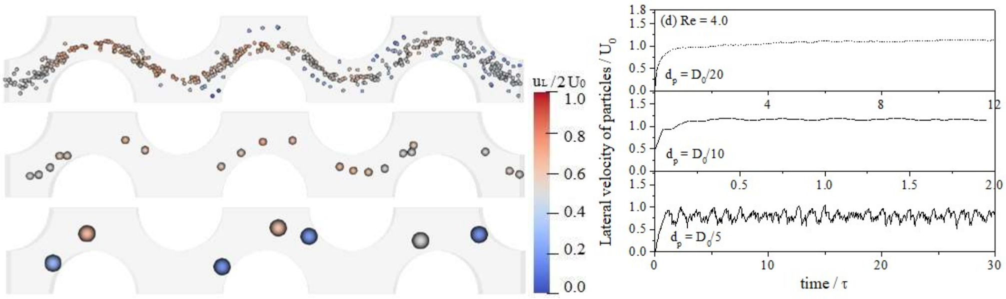

(c) Re = 4.0 (d) lateral averaged velocity of particles varying with time

Figure 4 Particle flow in porous media when the volume fraction of particles = 5.0%, W= 2.0 D_0, d_p = $D_0/20$, $D_0/10$, and $D_0/5$.

Figure 4 (a) to (c) present the instantaneous distribution of particles in the pseudo-steady state. Most particles moved along the center line of the wave channel in the form of a particle belt. The higher the slurry velocity is, the thinner the belt is. The bias of the large particles from the center path in Figure 4-(c) is due to its higher inertia.

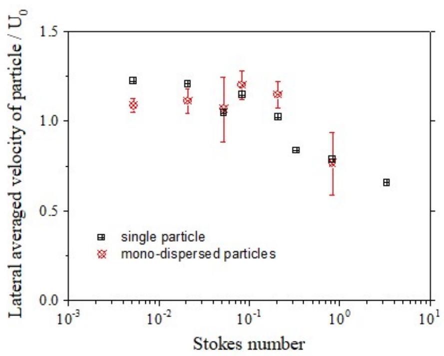

Figure 5 Lateral averaged velocity of particles varying with St, $W = 2.0\ D_0$.

Figure 5 calculated the lateral averaged velocity of particles varying with the stokes number. As the stokes number increased, the lateral velocity of particles reduced. The higher inertia of particles reduced the carrying capability of the liquid. Therefore, the lateral velocity of particles reduced accordingly. In addition, Figure 5 compared the averaged velocities of the multiple particles with those of single particles carried by the liquid. The lateral velocities of the single particle were close to those of multiple particle flow at the volume fraction of 5%. The inter-particle collision was little for the multiple particle flow at the volume fraction of 5%.

3.3 Volume fraction of particles

The effect of the volume fraction of particles on the particle clogging was studied by increasing the volume fraction of particles, α_s, from 5.0%, 10.0%, and 20.0% to 40.0%. Figure 6 shows the instantaneous distribution of particles in the porous medium when the particle diameters increased from (a) $D_0/20$, (b) $D_0/10$, to (c) $D_0/5$. In these figures, most particles were also distributed near the center path of the channel. As the volume fraction of particles increased, the particle belts widened. The particle velocity near the center line was simulated higher than that of particles near the porous medium. In Figure 6-(a), the particles at the diameter of $D_0/20$ were able to pass through the channel carried by the liquid at all these volume fractions.

In Figure 6-(b) and (c), the particles were trapped in the channel under the condition with a higher volume fraction of particles. The $D_0/10$ particles were trapped in the channel when the volume fraction raised to 40%, and the $D_0/20$ particles were trapped when the volume fraction was 20% and 40%. The multiparticle bridging was found to be built and trapped the particles in the porous media, by which the local volume fraction was increased behind the bridging front.

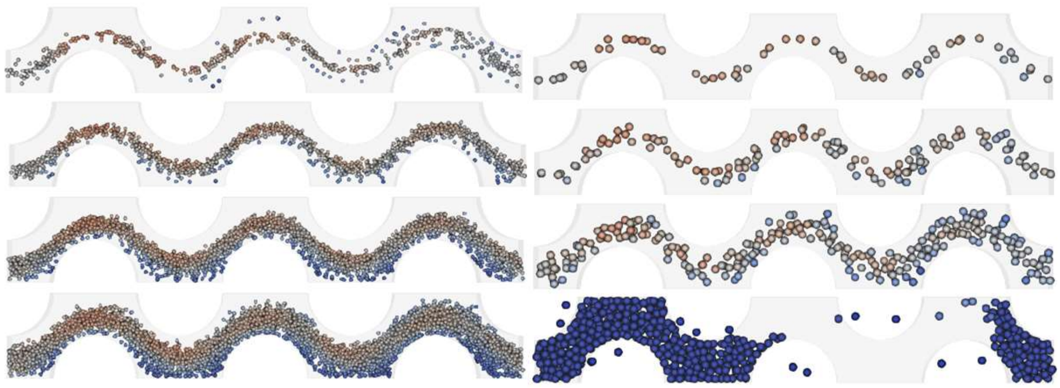

(a) d_p =D$_0$/20 (b) d_p =D$_0$/10

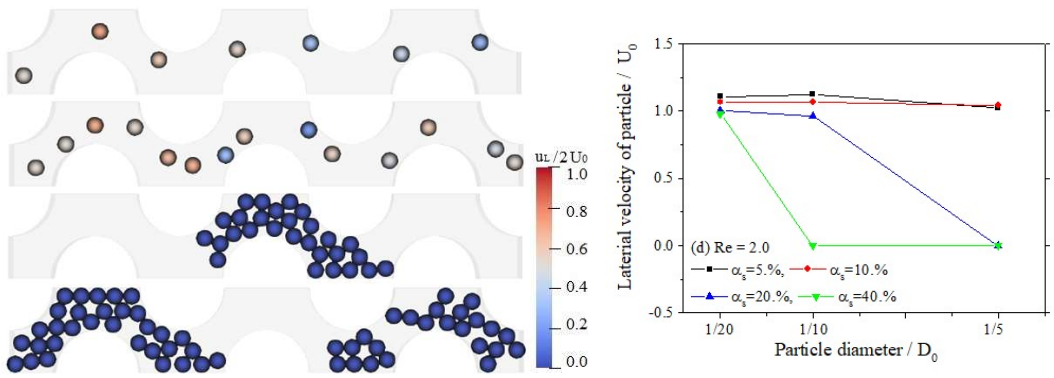

(c) d_p =D$_0$/5 (d) particle velocity affected by volume fractions

Figure 6. Particle flow affected by the volume fraction of particles. From top to bottom α_s = 5.0%, 10.0%, 20.0% and 40.0%

Figure 6-(d) shows the lateral averaged velocity of particles affected by the volume fraction of particles in the porous media. It is observed that the lateral velocity of smaller particles was higher than that of the large particles with all the volume fractions of particles. When the volume fraction of particles increased, the particle velocity reduced accordingly when some of the particles moved aside the center line of the wave channel, where the fluid velocity was lower near the surface of the porous medium. When α_s = 40%, the velocities of particles at the diameter of D$_0$/10 and D$_0$/5 reduced to zero as the particles were trapped in the porous media. At the same mass flow rate of the slurry, the particle velocity reduced when the volume fraction of particles was increased.

3.4 Particle clogging

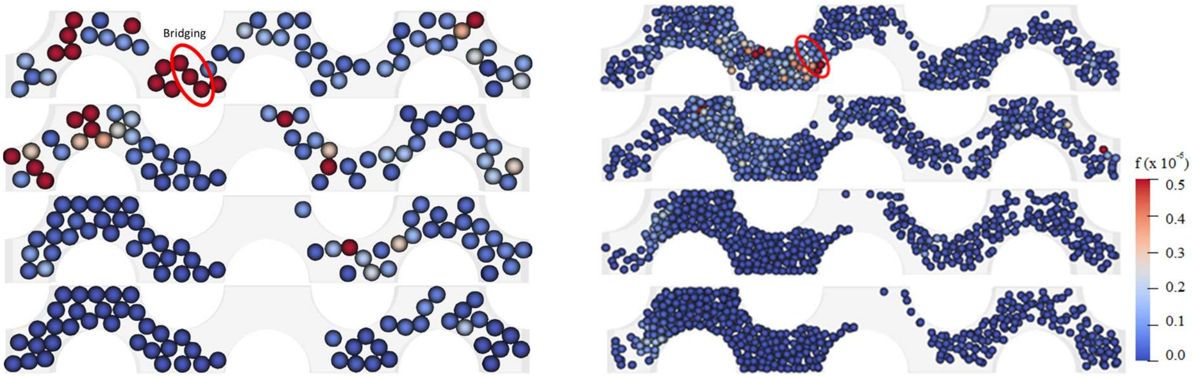

(a) d_p = 1/5 D_0, dt = τ. (b) d_p = 1/10 D_0, dt = τ

Figure 7. Distribution of particles varying with time when clogging. α_s = 40%

Figure 7 presents the distribution of particles when the multiparticle bridges were formed. The volume fractions of particles were both 40.0%. From top to bottom, the figure shows the evolution of the particle distribution varying with time. The time interval was τ. The colour of particles represents the magnitude of the force acting on themselves. On the top of Figure 7-(a), the red circle labelled the location where the bridge was formed. When moving toward the pore throat, the four particles circled were trapped, then built the bridge. The interaction between these particles increased the instantaneous force acting on each particle trapped. Meanwhile, the momentum loss of each particle generated additional force on particles impacted by the porous media surface. At the next time step, the forces on coming particles increased when hitting on the particle trapped in the wave channel. As the time varied, the kinetic energy from the coming particles wasn't high enough to break the bridge, which resulted in more particles trapped throughout the porous medium. This mechanism is also observed in the distribution of 1/10 D_0 particles in figure (b), where a larger number of the smaller particles formed the bridge.

Figure 8 shows the particle velocity varied with time when the particles were trapped in the porous media. Initially, the particles were accelerated, then the averaged velocity of particles reduced gradually until the velocities of all particles turned to zero when they were all trapped in the porous media. When d_p = 1/5 D_0, the particles in the high-volume fraction were trapped earlier. Comparing velocities of two sizes of particles at the same volume fraction of 40%, the large particles at 1/5D_0 were fully stopped earlier. These simulations evidenced that the critical condition of the particle clogging in the wave channel of the porous media existed when the particle size was large, meanwhile, the volume fraction of particles was high.

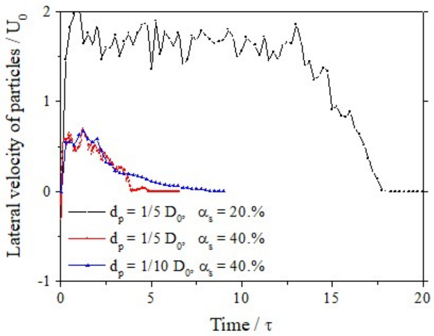

Figure 8. Particle velocities varied with time when clogging occurred.

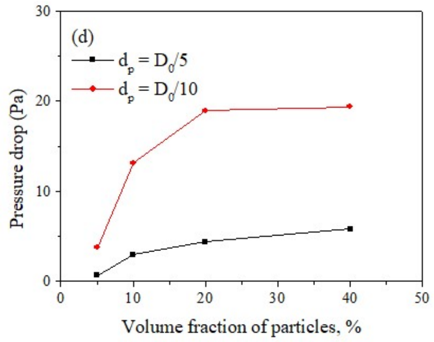

Figure 9. Total pressure drop and volume fraction of particles.

The particle clogging increases the volume fraction of particles and reduces the permeability by increasing the local static pressure. Figure 9 shows the total pressure drop of the porous media varied with the volume fraction and diameter of particles in the studies of Figure 6. The particle diameters were $D_0/5$ and $D_0/10$. The predicted pressure drops of both sizes of particles increased when the volume fraction of particles increased. The pressure drop created by the presence of the smaller particles at the diameter of $D_0/10$ was simulated higher than that by the larger particles when their initial volume fractions of particles were the same.

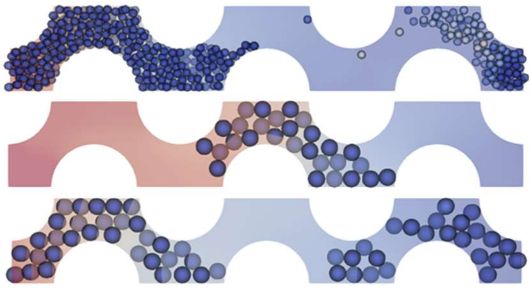

Figure 10. Pressure distribution when particle clogging occurred. From top to bottom, (a) $d_p = D_0/10$, $\alpha_s = 40\%$; (b) $d_p = D_0/5$, $\alpha_s = 20\%$; (b) $d_p = D_0/5$, $\alpha_s = 40\%$

Figure 10 shows the pressure distribution when the particles were trapped at the pore throat. The middle figure shows the pressure distribution when $d_p = D_0/5$ and $\alpha_s = 20\%$. It is seen that the particles were trapped in the middle of the porous media. On both the left and right sides of the particles, the pressure drops were much less than that in the particle-clogging region.

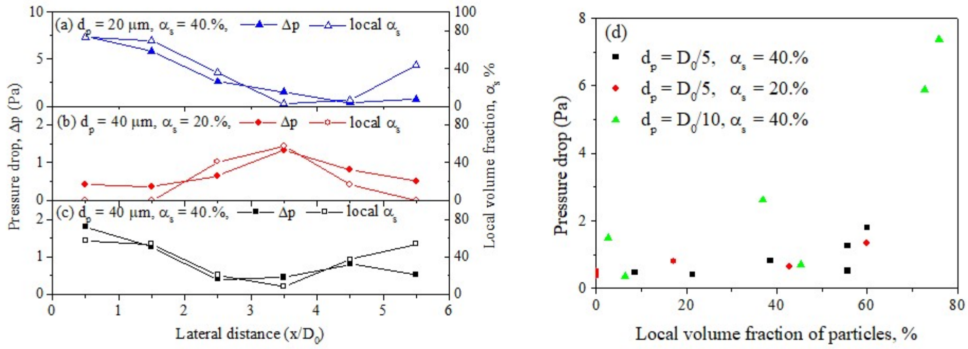

Figure 11. Local pressure drop and volume fraction of particles when particle clogging.

Figure 11 calculated the pressure drop along the lateral direction of the channel in Figure 10. It is observed in figure (b) that the pressure drop where $x/D_0 = 3\sim4$ was much highest, where the calculated volume faction of particles was also higher than that in other regions. In Figure 11-(a) and (c), the particles were trapped at the left and right sides of the channel. The volume fractions in these regions were predicted highest, where the pressure drop was also raised. The simulation result shows evidence that the local static pressure was raised by the particle clogging at the pore throat.

The relation between the local pressure drop and the volume fraction of particles is presented in Figure 11-(d). Among these simulation results with particle clogging, the local pressure drop raised with the increment of the local volume fraction of particles. The values of the local pressure drop in the system built with the smaller particles were higher than that with larger particles, when their local volume fractions were equal. Comparing the two conditions of various volume fractions of the large particles, when (a) $d_p = D_0/5$, $\alpha_s = 20\%$; and (b) $d_p = D_0/5$, $\alpha_s = 40\%$, their local pressure drop varies with the volume fraction of particles was discovered in a close relation. Therefore, particle clogging occurs when the local volume fraction increases to a condition where particle bridging can form. The pressure drop due to particle clogging is determined by the size and volume fraction of particles.

4. Conclusions

In this study, the liquid-particle flow was simulated using the CFD-DEM method to investigate the non-straining scheme of the particle filtration in porous media, where the particle diameter was smaller than the pore throat and the particle clogging was mainly due to the multiparticle bridging at the pore throat in porous media. The flow dynamics of the single particle and mono-sized multi-particle flow in slurry were simulated to study the effect of the volume fraction of particles on the particle clogging due to bridging and characterize the flow dynamics of fluid-particle motion when clogging occurred in porous media.

When Re < 1 and St << 1, the particle flow in the porous medium was dominated by the flow carrier and the particle's flow path and velocity followed the dynamics of the liquid in the porous media. As the Re increased and St increased to over 1, the larger particles were simulated moving slower than the liquid flow and/or biasing from the flow path of the liquid. The inertia of particles dominated the particle flow when St >1.

The particle clogging in porous media was predicted when the volume fraction of particles was high, and the ratio of the particle diameter to the size of the porous throat was large at 0.25 ~ 0.5. At the clogs, the coming particles were trapped behind the particle bridge and increased the volume fraction of particles locally, where the local static pressure was predicted to jump suddenly which increased the permeability of the porous media eventually. From the microscale simulation, particle clogging due to bridging occurs when St > 1, meanwhile, the local volume fraction of particles increases on the condition that particle bridging can form.

Reference

1 A. Zamani, B. Maini. Flow of dispersed particles through porous media — Deep bed filtration. Journal of Petroleum Science and Engineering 69 (2009) 71–88

2 R.N. Sacramento, Y.L. Yang, Z.J. You, A. Waldmann, A.L. Martins, A.S.L. Vaz, P.L.J. Zitha, P. Bedrikovetsky. Deep bed and cake filtration of two-size particle suspension in porous media. Journal of Petroleum Science and Engineering 126(2015) 201–210

3 M.T. Vu, A. Jardani, M. Krimissa, P. Fischer, N. Ahfir. Hydraulic tomography in time-lapse mode for tracking the clogging effects associated with the colloid injection. Advances in Water Resources 133 (2019) 103424

4 D.H. Kim, C. Lee, C. Choi, S.J. Ahn, I.S. Kim. Transport analysis of particulate matter in media-saturated mesh tube filter for the desalination primary pretreatment process. Desalination 495 (2020) 114642

5 D.Y. Lee, G.W. Lee, K. Yoon, B. Chun, H.W. Jung. Lattice Boltzmann simulations for wall-flow dynamics in porous ceramic diesel particulate filters. Applied Surface Science 429 (2018) 72–80

6 K. Yamamoto, S. Satake, H. Yamashita, N. Takada, M. Misawa. Lattice Boltzmann simulation on porous structure and soot accumulation. Mathematics and Computers in Simulation 72 (2006) 257–263.

7 Y. Xie, Y. Wang, M. Huo, Z. Geng, W. Fan. Risk of physical clogging induced by low-density suspended particles during managed aquifer recharge with reclaimed water: Evidences from laboratory experiments and numerical modelling. Environmental Research 186 (2020) 109527.

8 J.H.D. Hampton, S.B. Savage. Computer modelling of filter pressing and clogging in a random tube network. Chemical Engineering Science, 48(1993) 160-161.

9 S,J. Vitthal, M.M. Sharma. A Stokesian Dynamics Model for Particle Deposition and Bridging in Granular Media. Journal of Colloid and Interface Science, 153(1992)

10 J.R. Valdes, J.C. Santamarina. Particle clogging in radial flow: microscale mechanisms. SPE J. 11(2006) 193–198

11 X. Chen, Z. Wu, Q. Cai, W. Cao. Effect of ultrasonic stimulation on particle transport and fate over different lengths of porous media. Journal of Hydrology 559 (2018) 972–983.

12 M.A. Endo Kokubun, A. Muntean, F.A. Radu, K. Kumar, I.S. Pop, E. Keilegavlen, K. Spildo. A pore-scale study of transport of inertial particles by water in porous media. Chemical Engineering Science 207 (2019) 397–409

13 J.S. Kim, P.K. Kang. Anomalous transport through free-flow-porous media interface: Pore-scale simulation and predictive modelling. Advances in Water Resources 135 (2020) 103467

14 A. Parvan, S. Jafari, M. Rahnama, S. Norouzi-Apourvari, A. Raoof. Insight into particle retention and clogging in porous media; a pore scale study using lattice Boltzmann method. Advances in Water Resources 138 (2020) 103530.

15 A. Parvan, S. Jafari, M. Rahnama, S. Norouzi-Apourvari, A. Raoof. Insight into particle detachment in clogging of porous media; a pore scale study using lattice Boltzmann method. Advances in Water Resources 151 (2021) 103888

16 J.D. Hyman, M. Dentz. Transport Upscaling under Flow Heterogeneity and Matrix-Diffusion in Three-Dimensional Discrete Fracture Networks. Advances in Water Resources 155 (2021) 103994

17 J. Su, G. Chai, L. Wang, W. Cao, Z. Gu, C. Chen, X.Y. Xu. Pore-scale direct numerical simulation of particle transport in porous media. Chemical Engineering Science 199 (2019) 613–627

18 F. Gray, J. Cen, S.M. Shah, J.P. Crawshaw, E.S. Boek. Simulating dispersion in porous media and the influence of segmentation on stagnancy in carbonates. Advances in Water Resources 97 (2016) 1–10.

19 M.S. Kermani, S. Jafari, M. Rahnama, A. Raoof. Direct pore scale numerical simulation of colloid transport and retention. Part I: Fluid flow velocity, colloid size, and pore structure effects. Advances in Water Resources 144 (2020) 103694

[20] M.M. Gibson, B.E. Launder. Ground effects on pressure fluctuations in the atmospheric boundary layer, Journal of Fluid Mechanics. 86(1978) 491–511.

[21] C. Goniva, C. Kloss, N.G. Deen, J.A.M. Kuipers, S. Pirker. Particuology 2012, 10, 582.

[22] CFDEM. https://www.cfdem.com/media/CFDEM/docu/CFDEMcoupling_Manual.html

[23] K.H. Leitza, M. O'Sullivan, A. Plankensteiner, T. Lichtenegger, S. Pirker, H. Kestler, L.S. Sigl. CFDEM modelling of particle heating and acceleration in cold spraying. International Journal of Refractory Metals & Hard Materials 73 (2018) 192–198.

[24] Z. Y. Zhou, S. B. Kuang, K. W. Chu. A. B. Yu. Discrete particle simulation of particle–fluid flow: model formulations and their applicability. J. Fluid Mech. 611(2010) 482–510.

[25] Z.Y. Zhou, S.B. Kuang, K.W. Chu, A.B. Yu. J. Fluid Mech. 2010, 661, 482.

[26] J. Ai, J.F. Chen, J.M. Rotter, J.Y. Ooi. Powder Technology 2011, 206, 269.